Structure and stability of a thioredoxin reductase from Sulfolobus solfataricus: A thermostable protein with two functions

ARTICLE *in* BIOCHIMICA ET BIOPHYSICA ACTA · MARCH 2009

Impact Factor: 4.66 · DOI: 10.1016/j.bbapap.2008.11.011 · Source: PubMed

8 AUTHORS, INCLUDING:

Alessia Ruggiero
Italian National Research Council
59 PUBLICATIONS **539** CITATIONS
SEE PROFILE

Mariorosario Masullo
Parthenope University of Naples
97 PUBLICATIONS **951** CITATIONS
SEE PROFILE

Paolo Arcari
University of Naples Federico II
111 PUBLICATIONS **1,407** CITATIONS
SEE PROFILE

Luigi Vitagliano
Italian National Research Council
151 PUBLICATIONS **2,952** CITATIONS
SEE PROFILE

Biochimica et Biophysica Acta 1794 (2009) 554–562

Contents lists available at ScienceDirect

Biochimica et Biophysica Acta

journal homepage: www.elsevier.com/locate/bbapap

Structure and stability of a thioredoxin reductase from *Sulfolobus solfataricus*: A thermostable protein with two functions

Alessia Ruggiero [a], Mariorosario Masullo [b,c], Maria Rosaria Ruocco [c], Pasquale Grimaldi [b,c], Maria Angela Lanzotti [d], Paolo Arcari [c,e], Adriana Zagari [a,d,e], Luigi Vitagliano [a,*]

[a] *Istituto di Biostrutture e Bioimmagini, CNR, Via Mezzocannone 16, I-80134 Napoli, Italy*
[b] *Dipartimento di Scienze Farmacobiologiche, Università degli Studi "Magna Graecia" di Catanzaro, Roccelletta di Borgia, I-88021 Catanzaro, Italy*
[c] *Dipartimento di Biochimica e Biotecnologie Mediche, Università degli Studi di Napoli Federico II, Via S. Pansini 5, I-80131 Napoli, Italy*
[d] *Dipartimento delle Scienze Biologiche, Sezione di Biostrutture, Università degli Studi di Napoli Federico II, Via Mezzocannone 16, I-80134 Napoli, Italy*
[e] *CEINGE Biotecnologie Avanzate s.c.a r.l., Via Comunale Margherita 482, I-80145 Napoli, Italy*

ARTICLE INFO

Article history:
Received 12 September 2008
Received in revised form 13 November 2008
Accepted 14 November 2008
Available online 6 December 2008

Keywords:
Oxidoreductase
Archaea
Protein function and stability
Cofactor binding
NADH oxidase

ABSTRACT

Recent investigations have demonstrated that disulfide bridges may play a crucial role in the stabilization of proteins in hyperthermophilic organisms. A major role in the process of disulfide formation is played by ubiquitous proteins belonging to the thioredoxin superfamily, which includes thioredoxins (Trx), thioredoxin reductases (TrxR), and disulfide oxidases/isomerases (PDO/PDI). Here we report a characterization of the structure and stability of the TrxR (*Ss*TrxRB3) isolated from the archaeon *Sulfolobus solfataricus*. This protein is particularly interesting since it is able to process different substrates (Trxs and PDO) and it is endowed with an additional NADH oxidase activity. The crystal structure of the wild-type enzyme, of its complex with NADP and of the C147A mutant provides interesting clues on the enzyme function. In contrast to what is observed for class II TrxRs, in the structure of the oxidized enzyme, the FAD binding site is occupied by a partially disordered NAD molecule. In the active site of the C147A mutant, which exhibits a marginal NADH oxidase activity, the FAD is canonically bound to the enzyme. Molecular modeling indicates that a FAD molecule can be accommodated in the site of the reduced *Ss*TrxRB3. Depending on the oxidation state, *Ss*TrxRB3 can bind a different cofactor in its active site. This peculiar feature has been related to its dual activity. Denaturation experiments followed by circular dichroism indicate that electrostatic interactions play an important role in the stabilization of this thermostable protein. The analysis of the enzyme 3D-structure has also provided insights into the bases of *Ss*TrxRB3 stability.

1. Introduction

Disulfide bridge is a widespread structural element of crucial importance for the structure and/or the function of a large number of proteins [1]. This motif provides covalent links between cysteine residues located in a variety of different structural contexts [1–4]. Proteins may contain, in their native state, permanent disulfide bridges, which essentially contribute to their overall stability and/or transient disulfide bridges, often associated with a catalytic role in enzymes involved in cell redox regulation.

For long time, it has been assumed that the reducing conditions of the cytoplasm were not compatible with the presence of proteins with cysteine residues in their oxidized form. Accordingly, proteins containing disulfide bridges were believed to be relegated to extra-cytoplasmatic environments [5]. This common belief has been recently undermined by the discovery that a large fraction of proteins of hyperthermophilic organisms present disulfide bridges [6–8]. Indeed, it has been suggested that disulfide bridges may provide a significant contribution to the thermostability of these proteins by compensating insufficient levels of electrostatic charge optimization [9].

The process of disulfide formation is not spontaneous but it is modulated by complex enzymatic systems. A major role in this process is played by ubiquitous proteins belonging to the thioredoxin superfamily, which includes enzymes such as thioredoxins (Trx), thioredoxin reductases (TrxR), and disulfide oxidases/isomerases (PDO/PDI) [10–13]. Trx is the major ubiquitous disulfide reductase responsible for keeping proteins in their reduced state. Trx is a substrate of TrxR, which provides the reducing equivalents necessary to regenerate the reduced state of Trx. These electrons originate from NADPH and are transferred *via* FAD to the disulfide of the active site of TrxR, which subsequently reduces its protein substrate. TrxRs are homodimeric proteins in which each monomer contains a FAD molecule. Although TrxRs have been isolated from organisms

Abbreviations: Trx, thioredoxin; TrxR, thioredoxin reductase; *Ss*TrxRB3, *S. solfataricus* TrxRB3; *Ec*TrxR, *E. coli* TrxR; *At*TrxR, *A. thaliana* TrxR; *Hp*TrxR, *H. pylori* TrxR; *Mt*TrxR, *M. tuberculosis* TrxR; FAD, flavin adenine dinucleotide; NADP, nicotinamide adenine dinucleotide phosphate; NAD, nicotinamide adenine dinucleotide

* Corresponding author.
E-mail address: luigi.vitagliano@unina.it (L. Vitagliano).

1570-9639/$ – see front matter © 2008 Elsevier B.V. All rights reserved.
doi:10.1016/j.bbapap.2008.11.011

belonging to all of the three domains of life, archaea, eubacteria and eukarya, differences among TrxRs isolated from different sources have emerged [14]. TrxRs isolated from eubacteria and lower eukarya have been extensively characterized. On the other hand, very limited information is available on TrxRs isolated from archaea.

Recently, the thioredoxin reductase activity of an enzyme [15], previously classified as a NAD(P)H oxidase [16], isolated from the hyperthermophilic archaeon *Sulfolobus solfataricus* has been described (*Ss*TrxRB3—sequence entry Q97W27). The analysis of the *S. solfataricus* genome [17] reveals that the thioredoxin system is particularly intricate in this organism. Indeed, the presence of an additional putative TrxR (*Ss*TrxRB2—sequence entry Q97V69) and the coexistence of two distinct thioredoxin genes (*Ss*TrxA1 and *Ss*TrxA2, sequence entry Q980E5 and Q97WI4, respectively) have been detected [15,18]. Furthermore, a protein (*Ss*TrxRB1—sequence entry Q97WJ5) lacking the CxxC motif but with a significant sequence identity with other TrxRs has been characterized [19]. *S. solfataricus* genome also presents two distinct genes encoding for thioredoxin-like proteins (*Ss*TrxA1 and *Ss*TrxA2). The expression and the characterization of these proteins has demonstrated that neither *Ss*TrxRB1 nor *Ss*TrxRB2 exhibit any reductase activity using *Ss*TrxA1 and *Ss*TrxA2 as substrates [15,18]. On the other hand, *Ss*TrxRB3 efficiently reduces *Ss*TrxA1 and *Ss*TrxA2 as well as the *E. coli* Trx [15]. This scenario is further complicated by the discovery that *S. solfataricus* PDO is a substrate for *Ss*TrxRs [18].

Structural characterizations of TrxR and Trx isolated from *S. solfataricus* are essential for identifying the partnerships and the role of the different subjects involved in redox regulation.

In order to elucidate structure–function and structure–stability relationships of the *Ss*TrxRB3 enzyme, combined crystallographic and spectroscopic analyses have been undertaken. Here we present the crystal structure of the enzyme, of its complex with NADP and of the C147A mutant (*Ss*TrxRB3.C147A). Collectively, these structures clearly indicate that the enzyme shows unusual cofactor binding modes. In addition, denaturation experiments followed by circular dichroism provide insight into the structural bases of the enzyme stability.

2. Materials and methods

2.1. Protein crystallization, data collection and structure determination

*Ss*TrxRB3 and its C147A mutant were purified as previously reported [20]. For MAD experiments a selenomethionine derivative was also prepared [21]. Large crystals of all these forms were grown using 12–15% (w/v) poly-ethylene glycol 2000 monomethyl ether, 0.1 M $(NH_4)_2SO_4$ and 50 mM sodium acetate (pH 4.6). To characterize the NADP binding to the protein, crystals of the *Ss*TrxRB3 were also grown by adding the cofactor to the crystallization conditions (NADP/protein molar ratio of 100:1). A detailed description of the crystallization conditions has been published elsewhere [21].

Diffraction data were collected at 100 K at ESRF (Grenoble, France) (beam-line ID29) and, occasionally, in-house, using a Rigaku 007HF rotating anode generator equipped with a CCD Saturn944 detector. Attempts to solve the structure by molecular replacement were not successful. The structure of *Ss*TrxRB3 was solved by MAD experiments performed on a SeMet derivative of the protein (see Ruggiero et al. for further details [21]). A set of initial phases was obtained using the program *SOLVE* [22]. Subsequent density modification with the program *DM* [23] produced an experimental electron density of excellent quality. Indeed, the program ARP/wARP [24] was able to trace automatically most of the enzyme structure.

2.2. Refinement

All structures were refined using the program CNS [25,26]. In all cases, the starting models were initially refined by rigid-body adjustment followed by simulated annealing. In these stages NCS restraints were also applied. Subsequently, positional and B-factor refinements were conducted. In these stages, the NCS restraints were progressively released. Refinement runs were followed by manual intervention using the molecular graphic program O [27] to correct minor errors in the position of the side chains. Water molecules were identified by evaluating the shape of the electron density and the distance of potential hydrogen bond donors and/or acceptors. The inspection of the maps clearly indicated, with the exception of few terminal residues, the electron density is well-defined for most of the residues of the proteins. The electron density is very well defined for the adenosine and phosphate moieties of all structures. In contrast, the isoalloxazine moiety is ordered only for the C147A mutant. The electron density of the NADP in its complex with *Ss*TrxRB3 also provides a clear picture of the cofactor binding site. Crystallographic and stereochemical statistics of the final models are reported in Table 1. The coordinates of the models and the experimental structure factors of *Ss*TrxRB3, *Ss*TrxRB3$(NADP)_2$, and *Ss*TrxRB3.C147A have been reported in the Protein Data Bank with the codes 3F8P, 3F8R, and 3F8D, respectively.

Table 1
Crystal data and refinement statistics

	Wild-type	Se-Met	C147A	NADP complex
Data collection statistics				
Space group	$P2_12_12_1$	$P2_12_12_1$	$P2_12_12_1$	$P2_12_12_1$
Cell parameters (Å)	a=76.77	a=76.66	a=76.58	a=76.87
	b=120.68	b=121.82	b=121.87	b=123.42
	c=126.86	c=127.82	c=127.84	c=127.43
Resolution (Å)	20.0–1.8 (1.86–1.80)	30–1.75 (1.81–1.75)	30.0–1.4 (1.40–1.45)	20.0–1.95 (2.02–1.95)
Completeness (%)	99.8 (98.4)	98.9 (99.1)	98.9 (91.7)	89.9 (73.5)
Unique reflections	108800	119303	231790	80365
R_{merge}	5.2 (31.2)	6.3 (25.1)	8.1 (32.6)	5.3 (33.9)
Mean I/σ(I)	22.3 (5.3)	18.1 (5.1)	32.9 (6.7)	12.7 (2.8)
Refinement statistics				
Resolution range (Å)	20.0–1.80	20.0–1.75	30.0–1.40	20.0–1.95
R_{factor}/R_{free}	0.200/0.237	0.227/0.249	0.206/0.226	0.208/0.257
No. of protein atoms	9464	9394	9394	9399
No. of water molecules	298	245	393	360
RMSD from target values				
Bonds (Å)	0.015	0.0062	0.010	0.012
Angles (°)	1.61	1.14	1.85	1.53

Values given in parenthesis refer to the highest resolution shell.

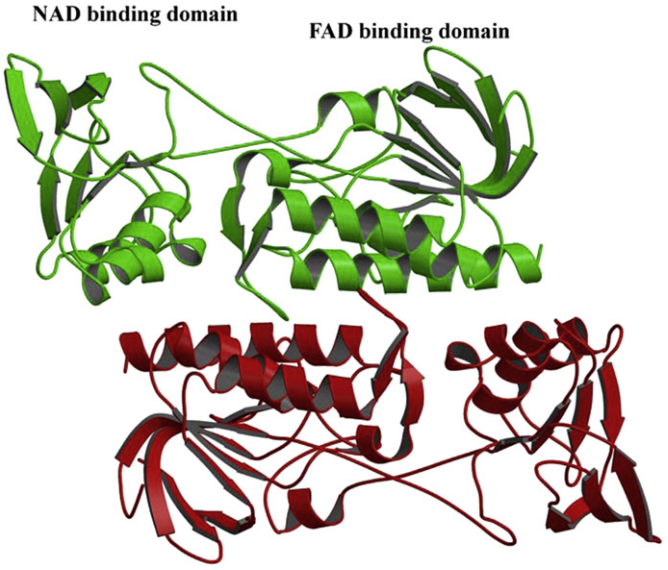

Fig. 1. Ribbon representation of *Ss*TrxRB3 dimer. The two monomers are colored in red and green (see the text for details).

2.3. Circular dichroism and denaturation experiments

*Ss*TrxRB3 CD spectra were recorded with a Jasco J-810 spectropolarimeter equipped with a Peltier temperature control system (Model PTC-423-S). Molar ellipticity per mean residue, $[\theta]$ in deg cm^2 dmol^{-1}, was calculated from the equation: $[\theta]=[\theta]$obs mrw $(10\ l\ C)^{-1}$, where $[\theta]$obs is the ellipticity measured in degrees, mrw is the mean residue molecular weight (108.5 Da), C is the protein concentration in g l^{-1} and l is the optical path length of the cell in cm. Far-UV measurements (185–250 nm) were carried out at 20 °C using a 0.1 cm optical path length cell and a protein concentration of 0.15 mg ml^{-1}. CD spectra, recorded with a time constant of 4 s, a 2 nm band width, and a scan rate of 5 nm min^{-1}, were signal-averaged over at least three scans.

Thermal denaturation curves were recorded over the 50–100 °C temperature range following the CD signal at 222 nm. The curves were registered using a 0.1 cm path length cell and a scan rate of 1.0 °C min^{-1}.

Chemical denaturation was carried out by treating the protein with either urea or guanidine hydrochloride (GuHCl). Both denaturants were purchased from Sigma. A commercial 8 M GuHCl solution was utilized. Stock solutions of urea and GuHCl, in different amounts, were mixed with protein solutions to give a constant final value of the protein concentration (0.15 mg ml^{-1}). The final concentration of urea and GuHCl was in the range 0.0–9.5 M and 0.0–6.0 M, respectively. All the chemical denaturation experiments were carried out in 20 mM sodium phosphate (pH 7.0) buffer after overnight incubation. The

```
                    10        20        30        40                50
Ss TrxRB3  MSLLPRTTSVKPGEKFDVIIVGLGPAAYGAALYSARYMLKTLVIGE------TPGGQLT
Ec TrxR    ---------MGTTKHSKLLILGSGPAGYTAAVYAARANLQPVLITG-----MEKGGQLT
Mt TrxR    -MTAPPVHDRAHHPVRDVIVIGSGPAGYTAALYAARAQLAPLVFEG-----TSFGGALM
Hp TrxR    --------------MIDCAIIGGGPAGLSAGLYATRGGVKNAVLFE----KGMPGGQIT
At TrxR    ------MNGLETHNTR-LCIVGSGPAAHTAAIYAARAELKPLLFEGWMANDIAPGGQLT

                   60        70        80        90       100       110
Ss TrxRB3  EAGIVDDYLGLIE-IQASDMIKVFNKHIEKYEVPVLLDIVEKIENRGDEFVVKTKRKGEF
Ec TrxR    TTTEVENWPGDPNDLTGPLLMERMHEHATKFETEIIFDHINKVDLQNRPFRL-NGDNGEY
Mt TrxR    TTTDVENYPGFRNGITGPELMDEMREQALRFGADLRMEDVESVSLHGPLKSVVTADGQTH
Hp TrxR    GSSEIENYPGVKEVVSGLDFMQPWQEQCFRFGLKHEMTAVQRVSKKDSHFVILAEDGKTF
At TrxR    TTTDVENFPGFPEGILGVELTDKFRKQSERFGTTIFTETVTKVDFSSKPFKLFT-DSKAI

                  120       130           140       150       160
Ss TrxRB3  KADSVILGIGVKRRKLGVPGEQEF----AGRGISYCSVCDAPLFK--NRVVAVIGGGDSA
Ec TrxR    TCDALIIATGASARYLGLPSEEAF----KGRGVSACATCDGFFYR--NQKVAVIGGGNTA
Mt TrxR    RARAVILAMGAAARYLQVPGEQEL----LGRGVSSCATCDGFFFR--DQDIAVIGGGDSA
Hp TrxR    EAKSVIIATGGSPKRTGIKGESEYW----GKGVSTCATCDGFFYK--NKEVAVLGGGDTA
At TrxR    LADAVILATGAVAKRLSFVGSGEASGGFWNRGISACAVCDGAAPIFRNKPLAVIGGGDSA

                 170       180       190       200           210           220
Ss TrxRB3  LEGAEILSSYSTKVYLIHRRDTFKAQPIYVETVKK---KPNVEFVLNSVVKEIKGD---K
Ec TrxR    VEEALYLSNIASEVHLIHRRDGFRAEKILIKRLMDKVENGNIILHTNRTLEEVTGD--QM
Mt TrxR    MEEATFLTRFARSVTLVHRRDEFRASKIMLDRARN---NDKIRFLTNHTVVAVDGD---T
Hp TrxR    VEEAIYLANICKKVYLIHRRDGFRCAPITLEHAKN---NDKIEFLTPYVVEEIKGD--AS
At TrxR    MEEANFLTKYGSKVYIIHRRDAFRASKIMQQRALS---NPKIDVIWNSSVVEAYGDGERD

                 230       240       250       260           270
Ss TrxRB3  VVKQVVVENLKTGE-IKELNVNGVFIEIGFDPPTDFAKSNGI----ETDTNGYIKVDE--
Ec TrxR    GVTGVRLRDTQNSDNIESLDVAGLFVAIGHSPNTAIFEGQL-----ELE-NGYIKVQSGI
Mt TrxR    TVTGLRVRDTNTGA-ETTLPVTGVFVAIGHEPRSGLVREAI-----DVDPDGYVLVQ---
Hp TrxR    GVSSLSIKNTATNE-KRELVVPGFFIFVGYDVNNAVLKQEDNSMLCKCDEYGSIVVD---
At TrxR    VLGGLKVKNVVTGD-VSDLKVSGLFFAIGHEPATKFLDGGV-----ELDSDGYVVTKP--

                 280       290       300       310       320
Ss TrxRB3  ---WMRTSVPGVFAAGDCTSAWLGFRQVITAVAQGAVAATSAYRYVTEKKGKK
Ec TrxR    HGNATQTSIPGVFAAGDVMDH--IYRQAITSAGTGCMAALDAERYLDGLADAK
Mt TrxR    -GRTTSTSLPGVFAAGDLVDR--TYRQAVTAAGSGCAAAIDAERWLAEHAATGEADSTD
Hp TrxR    --FSMKTNVQGLFAAGDIRIF--APKQVVCAASDGATAALSVISYLEHHALIGAQR
At TrxR    --GTTQTSVPGVFAAGDVQDK--KYRQAITAAGTGCMAALDAEHYLQEIGSQQGKSD
```

Fig. 2. Multiple sequence alignment of the Class II TrxRs whose three-dimensional structure has been solved. The numbering refers to *Ss*TrxRB3. Regions corresponding to α-helices, 3_{10} helices and β-sheets are colored in magenta, yellow and cyan, respectively.

urea- and GuHCl-induced denaturations were investigated by CD spectroscopy.

3. Results

3.1. Overall quality of SsTrxRB3 structures

The structure of the thermostable *Ss*TrxRB3 was determined by MAD using the SeMet derivative of the enzyme. For all forms (wild-type, C147A mutant, and NADP complex) the electron density maps are extremely well-defined for most of the residues. Disordered residues are located at the N- (1–10) and C-terminal ends (319–324) of the enzyme. Weak or absent electron density is also detected for residues of the loop region 97–100. The stereochemical parameters of the refined structures are in line with those reported for well-refined structures.

3.2. Wild-type SsTrxRB3 structure

The asymmetric unit of the $P2_12_12_1$ crystals contains two distinct copies of the protein dimer, which represents the biologically functional unit of the enzyme (Fig. 1). Each monomer consists of 324 residues and displays a sequence identity of ~35–40% with the eubacterial/eukaryal counterparts with known structures (Fig. 2). The overall structure of the four monomers in the asymmetric unit is virtually identical, with root mean square deviations (RMSD) falling into the interval 0.5–0.7 Å. On analogy with TrxRs previously characterized [28–33], each monomer has two distinct domains: the FAD-binding (residues 10 to 121 and 249 to 324) and the NADP-binding domain (residues 122–248) both displaying a nucleotide-binding fold. The FAD domain has an α/β structure composed of a central β-sheet flanked on the side by three parallel α-helices and on the other side by a three-stranded β-sheet. As expected for this class of proteins [34], the NADP-binding domain is smaller, although structurally related to the FAD-binding domain. The analysis of the B factors of the two domains suggests that the FAD domain is more rigid than the NADP one. Indeed, the average B-factor for the monomer A, which presents the best defined electron density, is 23.9 and 11.5 $Å^2$ for the NADP and FAD domain, respectively. Similar trends are observed for the other copies of the asymmetric unit. This finding is in line with the overall architecture of *Ss*TrxRB3 dimer (Fig. 1), whose interface mainly involves the FAD domain. Evidently, the contacts of the FAD domain at this interface reduce its flexibility.

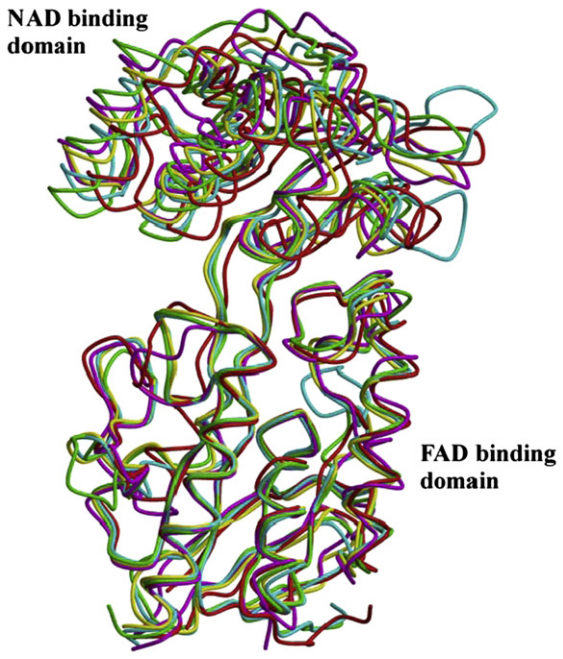

Fig. 3. Superimposition of the *Ss*TrxRB3 monomer (red) with that of *Hp*TrxR (magenta), *At*TrxR (cyan), *Ec*TrxR (green) and *Mt*TrxR (yellow). Residues of the FAD domain have been used for the superimposition.

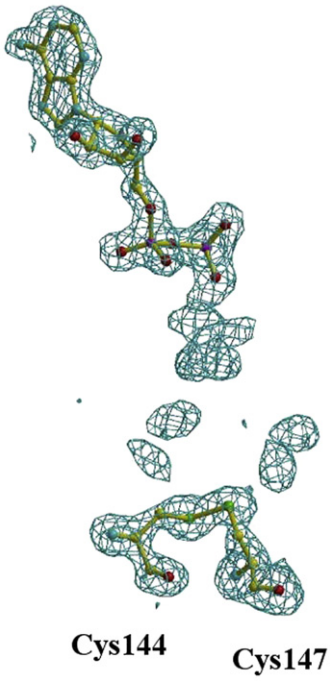

Fig. 4. Omit Fo-Fc map (countered at 2.5 σ) of the cofactor bound to expected FAD binding site of wild-type *Ss*TrxRB3. The residues of the disulfide bridge (Cys144–Cys147) are also shown.

The comparison of the overall structure of the monomers suggests that the relative orientation of the two domains found in *Ss*TrxRB3 is significantly different from that exhibited by the eukaryal TrxRs with known structure (Fig. 3). Indeed, while the monomers of *E. coli* (*Ec*TrxR) [28,32] and *Arabidopsis thaliana* (*At*TrxR) [32] TrxR exhibit an RMSD value, computed on the C^{α} atoms, of 1.0 Å, analogous comparisons of *Ss*TrxRB3 monomers with those of *Ec*TrxR and *At*TrxR produce larger deviations (RMSD ~1.4 Å). Similarly, the structure of *Helicobacter pylori* (*Hp*TrxR) [33] and *Mycobacterium tuberculosis* (*Mt*TrxR) [29] TrxR is closer to *Ec*TrxR and *At*TrxR than to *Ss*TrxRB3. These differences, along with the presence of multiple copies of the monomer in the asymmetric units, may also explain the difficulties met in the molecular replacement trials and the necessity to resort to MAD experiments.

3.3. Cofactor binding to wild-type and SsTrxRB3.C147A: a puzzling issue

In the initial characterization, no external cofactor was added to the crystallization medium to verify the intrinsic propensity of the enzyme to bind the cofactors NAD/NADP and FAD. The analysis of the expected NADP binding site in the structure of both wild-type and SeMet derivative of *Ss*TrxRB3 did not reveal the presence of the cofactor. Indeed, sulfate molecules are located in the pocket that should have been occupied by the nucleotide. This is not unexpected as ammonium sulfate was present in the crystallization medium.

Since the structures of *Ss*TrxRB3 and SeMet *Ss*TrxRB3 have been determined from crystals grown in air atmosphere, it is not surprising that the two cysteine residues of the active site (Cys144 and Cys 147) form a disulfide bridge. As shown in Fig. 4, these residues present a very well-defined electron density as most of the other active site residues. More problematic has been the interpretation of the electron

density corresponding to the cofactor bound at the enzyme active site. In the elongated shape of the density there are some groups that can be clearly identified (Fig. 4). In particular, the adenine, the ribose, and the pyrophosphate moieties are very well defined. Some extra electron density, linked to the pyrophosphate group, is also present. The quality of this portion of the density does not allow an unambiguous identification of the chemical nature of this part of the molecule. However, the shape of the density seems to correspond to a cyclic group rather than to the linear ribityl moiety of the FAD. Finally, scarce electron density is detectable in the cavity canonically deputed, in class II TrxRs, to the anchoring of the isoalloxazine moiety of the FAD. This picture invariantly emerges from the analysis of the active site of the four independent *Ss*TrxRB3 monomers present in the asymmetric unit. A virtually identical distribution of the electron density emerges for the analysis of the selenio-methionine derivative of *Ss*TrxRB3 (data not shown). Spectroscopic experiments aimed at quantifying the FAD present in the solutions used for the crystallization experiment suggests that the cofactor/protein ratio was only ~0.25. Taking into account that the ADP moiety of the cofactor bound to the enzyme could be straightforwardly refined with a full occupancy, this finding provides indirect evidence that the molecule located at the enzyme active site cannot be FAD. Crystals of the enzyme were also grown by adding exogenous FAD in a protein/cofactor molar ratio of 1:10. Structural analyses performed on diffraction data collected on these crystals confirmed the scenario emerged from the previous investigations without any significant modification of the electron density at the active site (Fig. S1, Supplementary material).

The structural characterization of other forms of the enzyme provided the clues required to solve this puzzling issue. Attempts to collect diffraction data on the reduced form of the enzyme were unsuccessful, due to severe crystal damage upon reduction. To obtain insight into the structural features of a non-oxidized form of the enzyme, we determined the structure of the mutant Cys147Ala (*Ss*TrxRB3.C147A), which, according to previous biochemical characterizations, displays only a marginal NADH oxidase activity [20]. Compared to wild-type, crystals of the mutant diffracted at significantly higher resolution (1.40 *versus* 1.80 Å). The overall structure of the mutant is essentially unchanged compared to the wild-type enzyme (RMSD value of the mutant *versus* the wild-type enzyme computed on the backbone atoms of the entire dimer is 0.38 Å). As expected, the local structure of the active site is perturbed by the mutation. The electron density is well-defined for all residues of the enzyme active site, including Cys144 and Ala147 (Fig. 5), which, in the wild-type oxidized enzyme, are involved in the disulfide bridge formation. Notably, in contrast to what found for the wild-type enzyme, the cofactor bound at the enzyme active site can be unequivocally identified as a FAD molecule since it exhibits a very clear electron density (Fig. 5, see Table S1 for H-bonding interactions established between FAD and protein atoms). This finding indicates that, upon mutation, the size of the isoalloxazine binding pocket increases thus allowing the correct positioning of the cofactor. The location of the isoalloxazine moiety in its canonical position also leads to a stabilization of the local structure of the enzyme. Indeed, in contrast to what observed for wild-type form, the side chain of the residue Gln51, which presents some mobility in the wild-type enzyme, shows a well-defined electron density and it is engaged in hydrogen bonding interactions with the side chain of Asp287. The presence of a tightly bound FAD cofactor at the active site may also account for the better diffraction power of the mutant crystals.

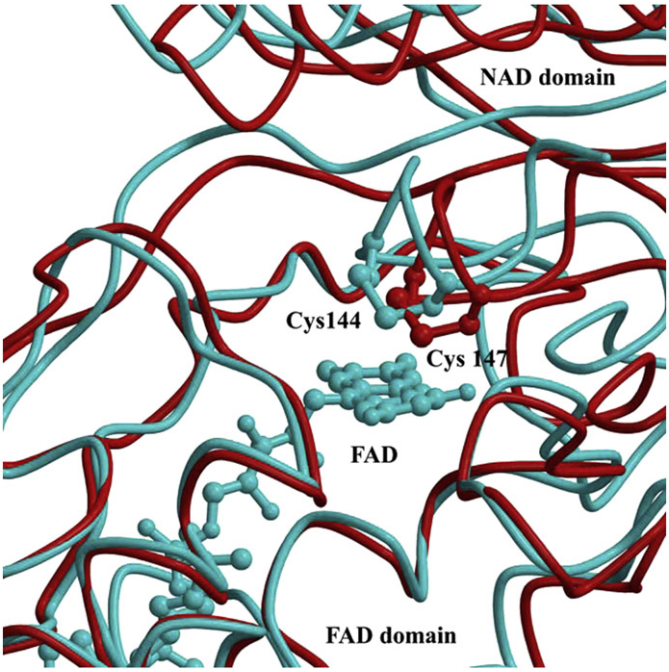

Fig. 6. Active sites of *Ss*TrxRB3 (red) and *Ec*TrxR (cyan). Residues of the FAD domain have been used for the superimposition. The location of the FAD cofactor of *Ec*TrxR and the active site disulfide bridges of the two enzymes are also shown.

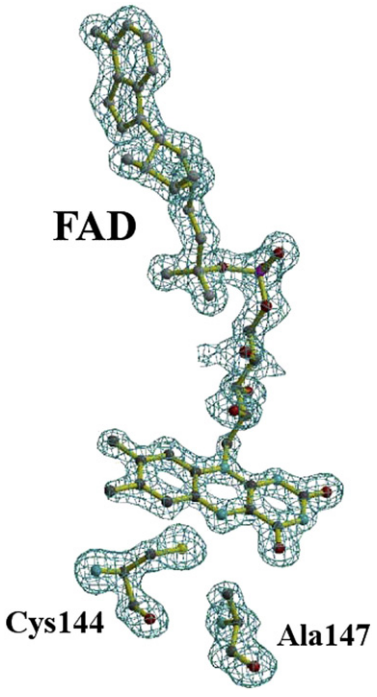

Fig. 5. Omit Fo–Fc map (countered at 3.0 σ) of the FAD molecule bound to *Ss*TrxRB3.C147A. The residues of the active site Cys144 and Ala147 are also shown.

The crystal structure of *Ss*TrxRB3.C147A, which exhibits a FAD cofactor bound in a canonical way, was used as a model to interpret the anomalous behavior of the wild-type enzyme. A molecular modeling session, carried using the conformation of the FAD moiety observed in the structure of the mutant, clearly indicates that the size of the isoalloxazine pocket of the oxidized wild-type enzyme is too small to accommodate this cofactor. Indeed, the positioning of the isoalloxazine ring within the pocket indicates that rather severe steric clashes occur. Among a number of short contacts (~3.2 Å), particularly critical is the clash between the S^{γ} of Cys147 side chain and the atom C4M of the FAD (2.95 Å). The overall size of the cavity also precludes alternative conformations of the FAD. These data suggest that the

oxidized state of the enzyme is not compatible with the binding of the FAD.

A comparison of wild-type *Ss*TrxRB3 structure with the oxidized forms of other class II TrxR provides some hints in the anomalous behavior of this enzyme. In particular, as shown in Fig. 6, the superimposition of *Ss*TrxRB3 and *Ec*TrxR FAD domains clearly indicates that the NAD domains are significantly displaced in the two enzymes. The variation of the relative orientation of the two domains brings the active site disulfide bridge of *Ss*TrxRB3 in a position which is incompatible with a canonical binding of the FAD ring (Fig. 6). It is important to note that in the mutant *Ss*TrxRB3.C147A, the relative orientation of the domains closely resembles the one detected in the wild-type enzyme. Therefore, the ability of *Ss*TrxRB3. C147A to bind the FAD cofactor is not due to a rearrangement of the relative orientation of the two domains but it results from the release of structural restraints upon disulfide bond breaking. A molecular modeling also indicates that the reduced form of the enzyme is able to productively bind FAD. Furthermore, this form should also be able to bind a reduced $FADH_2$ molecule in the conformation found in *H. pylori* TrxR [33].

A clear and conclusive indication on the chemical nature of the nucleotide bound was serendipitously obtained in the characterization of NADP binding to the oxidized *Ss*TrxRB3. Since, as mentioned before, in wild-type *Ss*TrxRB3 the NADP binding site is occupied by sulfate ions we have co-crystallized the enzyme with a large excess of NADP (*Ss*TrxRB3/NADP molar ratio 1:100). The analysis of the electron density maps derived from data collections performed on these crystals clearly indicate that the binding of NADP to *Ss*TrxRB3 closely resembles that found in the structure of *Ec*TrxR (Fig. 7). As in *Ec*TrxR, this site is rather distant from the active site of the enzyme. The electron density is well defined for the ADP moiety, whereas the nicotinamide group of the NADP is somewhat disordered. Particularly important is the role played by interactions of charged residues of the protein with 2′-phosphate group of the cofactor. Surprisingly, we noticed that the electron density at active site of the enzyme also showed a significant modification. Although the densities for the adenine, the ribose, the pyrophosphate moieties are conserved, there is a strong extra peak linked to the 2′ oxygen atom of the ribose. The shape and the location of the density clearly indicate that it corresponds to a phosphate group linked to the adenine ribose. The obvious interpretation of this unexpected finding is that a NADP molecule is also bound at the active site. This structure therefore corresponds to a *Ss*TrxRB3$(NADP)_2$ complex, with two bound NADP molecules adopting rather different conformations (Fig. 7). The strict analogy (Figs. 4 and S2), with the exception of the extra 2′ phosphate group, of the electron density at active sites of wild-type *Ss*TrxRB3 and *Ss*TrxRB3$(NADP)_2$ strongly indicates that a NAD molecule is bound to wild-type *Ss*TrxRB3. The small size of the nicotinamide and the absence of specific anchoring points in the cavity for this base render this part of NAD mobile in the complex, although, as shown in Fig. S2, some extra electron density is present in the cavity. Along this line, our data demonstrate that the oxidized form of the enzyme prefers a partially disordered NAD cofactor to the standard FAD cofactor.

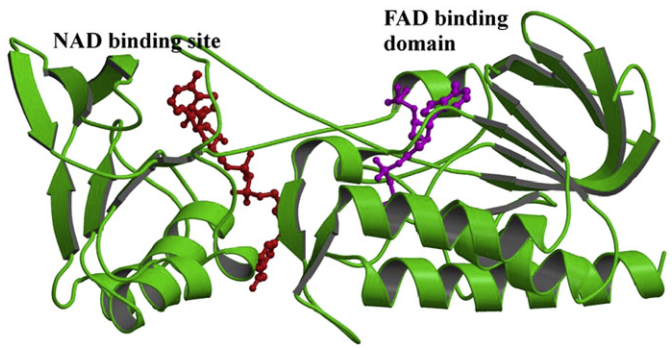

Fig. 7. Structure of *Ss*TrxRB3 in complex with two molecules of NADP. NADP molecules bound to the NAD binding site and to the enzyme active site are colored in red and magenta, respectively.

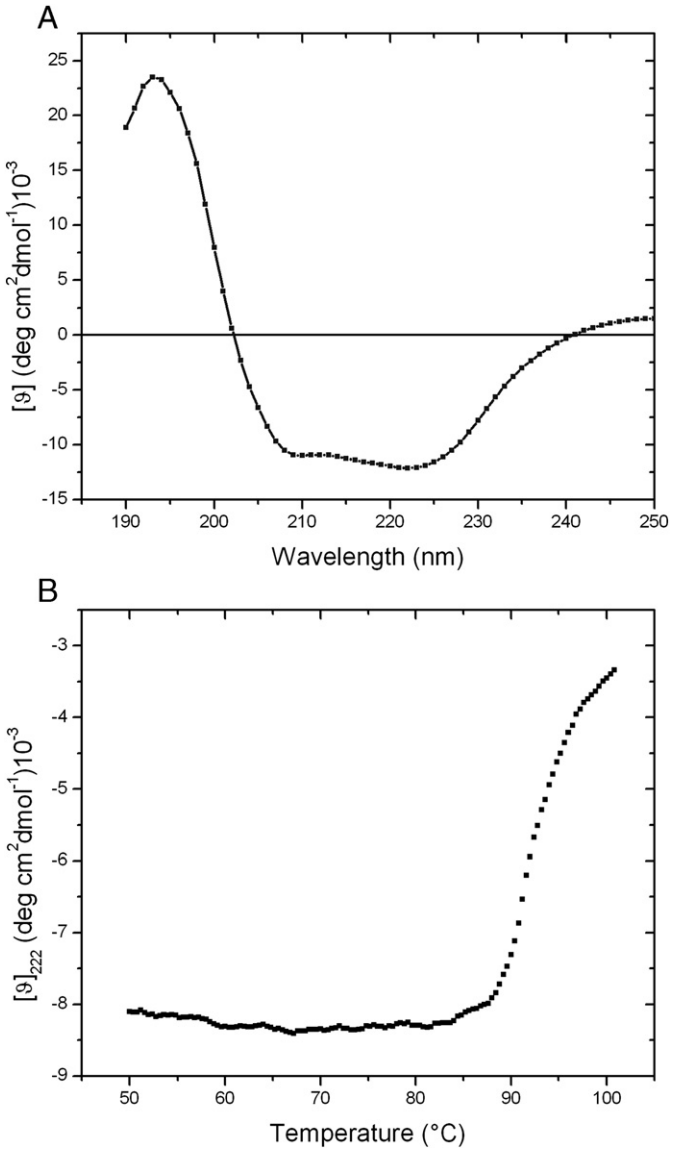

Fig. 8. Spectroscopic characterization of *Ss*TrxRB3: far-UV CD spectrum (A) and the thermal denaturation curve (B).

3.4. Chemical stability of SsTrxRB3 analyzed by circular dichroism

Circular dichroism spectra of *Ss*TrxRB3 were recorded at 20 °C in the far-UV region (Fig. 8). The maximum centered at 195 nm and the broad minimum centered at 222 nm in far-UV CD spectra of *Ss*TrxRB3 are indicative of the presence of both α and β secondary structure elements. A quantitative estimation of the secondary structure content, performed by using the self-consistent method [35], shows that the α-helix and the β-sheet contents are ~37% and 38%, respectively. These values are in line with those derived from the X-ray structure (α-helix and β-sheet content of ~30% and 36%, respectively). Thermal denaturation experiments indicate that at high temperature protein unfolding is associated with aggregation (Fig. 8B). Although this observation prevents any characterization of

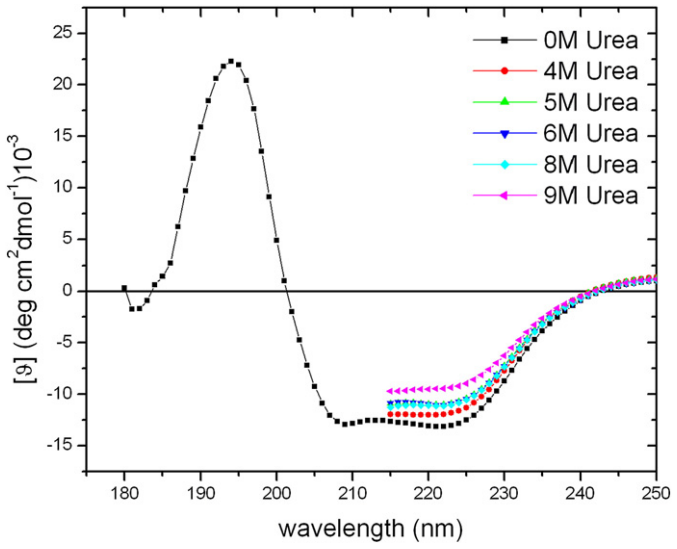

Fig. 9. Far-UV CD spectra of the native *Ss*TrxRB3 treated with urea solution at different concentrations.

the unfolding process of the enzyme, the appearance of the CD spectra at high temperature (80–85 °C), which closely resemble those collected at room temperature, confirms that the protein is thermostable.

The conformational stability of *Ss*TrxRB3 against the denaturing action of either urea or GuHCl was investigated by recording CD spectra as a function of the denaturant concentration. The analyses of the spectra collected in the presence of urea indicate that the protein is very stable against this denaturant agent (Fig. 9). Indeed, the evolution of the spectra upon addition of urea indicates that the secondary structure elements of the protein are well preserved even at concentrations of the denaturant as high as 9 M.

A rather different picture emerges from the denaturation experiments performed by using GuHCl. As shown in Fig. 10, even moderate amounts of GuHCl (~2.5 M) have a dramatic impact on the structure of the enzyme. Moreover, at high concentration of GuHCl the molar ellipticity of *Ss*TrxRB3 is close to zero. This is an indication that the unfolded state does not contain residual secondary structure. The relatively low (2.9 M) $[GuHCl]_{1/2}$ value (denaturant concentration at half-completion of the transition) indicates that electrostatic interactions play an important role in the stabilization of *Ss*TrxRB3 [36].

4. Discussion

All living organisms have developed efficient systems for scavenging reactive oxygen species generally produced by metabolism. The thioredoxin system, composed by thioredoxin, thioredoxin reductase, and NADPH plays a pivotal role in maintaining the redox state of the cell and in protecting the cell against oxidative stress. Recent investigations have also shed light on the importance of this system in hyperthermophilic organisms since disulfide formation is a widespread process for the stabilization of proteins even in intracellular environments [6,7,37]. However, structural information on these proteins is so far very limited. Here we report crystallographic and spectroscopic characterizations of the enzyme *Ss*TrxRB3 which is able, as a thioredoxin reductase, to process different substrates (thioredoxins and PDO) [15,18,20] and is also endowed with a NADH oxidase activity [16]. The structural characterization of the wild-type enzyme has shown a peculiar binding mode of its cofactors (NAD, NADP, and FAD). Indeed, although the overall organization of the enzyme follows the scheme emerged from the analyses of the eukaryal/eubacterial class II TrxRs, *Ss*TrxRB3 is unable to bind the FAD cofactor in its oxidized form. Due to the peculiar relative orientation of the FAD and NADP domains of the protein, the formation of the disulfide bridge at the active site reduces the size of the FAD cavity to an extent that precludes the binding of the cofactor. This favors the binding of NAD (and likely NADH) to wild-type *Ss*TrxRB3 in its oxidized state, that is anchored through its ADP moiety. On the other hand, the C147A mutant and presumably the reduced *Ss*TrxRB3 form productively bind the FAD cofactor at the active site. Therefore, depending on the oxidation state of the enzyme CxxC motif, *Ss*TrxRB3 can bind a different cofactor in its active site. Obviously, the inability of the oxidized form of *Ss*TrxRB3 to bind the FAD cofactor does not represent an impediment to the TrxR activity. Indeed, the reduction of the active site disulfide bridge and the conformational transition of the enzyme upon the binding of large substrates (Trx and PDO) can easily increase the size of the cavity, thus allowing a productive FAD binding. The steric hindrance produced by the FAD binding to the oxidized enzyme may also facilitate, in the presence of Trx/PDO substrates, conformational switches that lead to the formation of functional complexes. Along this line, also small substrates that are effectively reduced by *Ss*TrxRB3 are also able to induce the structural modifications required to productively bind the FAD cofactor.

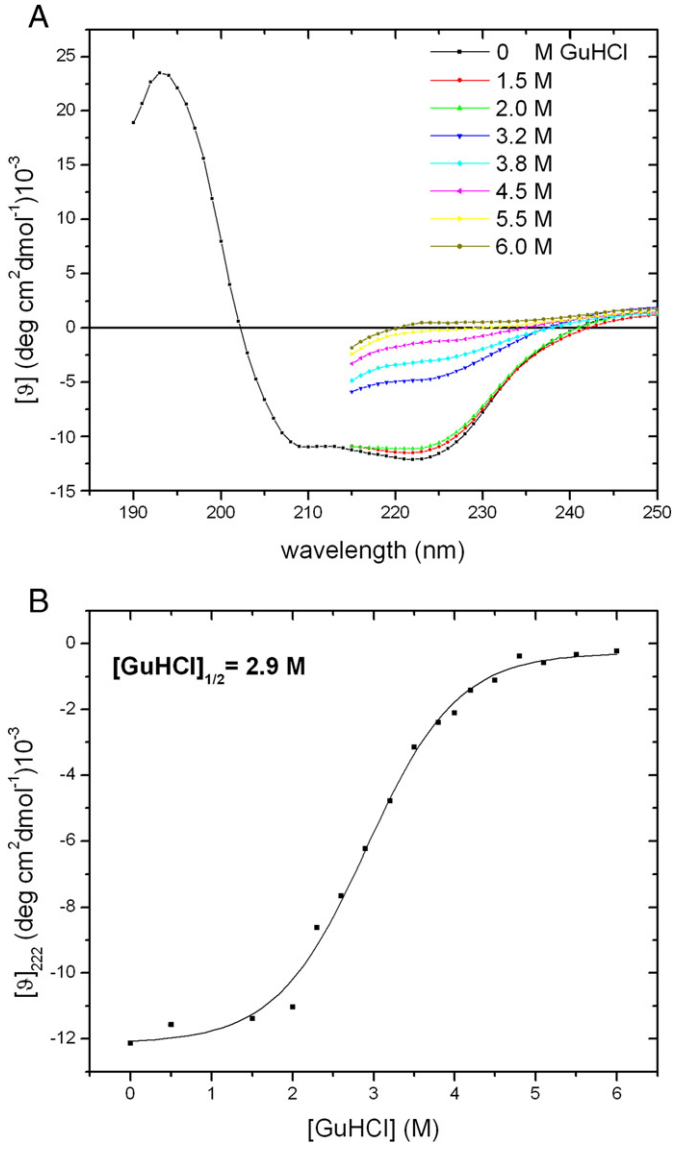

Fig. 10. Far-UV CD spectra of the native *Ss*TrxRB3 treated with different concentrations of GuHCl (A). In panel B the values of θ at 222 nm are reported as function of GuHCl concentration.

Although *Ss*TrxRB3 in its thioredoxin reductase function binds FAD and NADP in a standard way, with both cofactors involved in the substrate reduction, the unusual location of the NAD in the FAD binding site observed in the oxidized form of the enzyme is likely related to the second function elicited by the protein: the NAD oxidase activity. Although the definition of the precise mechanism of the NADH oxidase activity is rather difficult, some possibilities may be proposed on the basis of the present findings. The simplest hypothesis is that the NADH binding to the enzyme is important to keep the cofactor in an extended conformation that is more prone to oxidation. Upon binding to the active site of *Ss*TrxRB3, the nicotinamide moiety of NAD is highly mobile as demonstrated by its disordered electron density and it can assume multiple alternative conformations. The nicotinamide base is also directly connected with the external solvent. Indeed, the cavity is limited by residues of the fragment 49–83, in addition to the region embedding active site Cys. The terminal ends of this fragment assume helical structure (residues 49–55 and 69–83 are in 3_{10} and α-helical conformation, respectively). This motif is stabilized by a short two-stranded β-sheet (residues 56–58 and 67–68). Notably, this latter element is present only in the structure of the eukaryal TrxR isolated from *A. thaliana*, whereas it is missing in all eubacterial TrxR structures so far reported. Side chains of the 3_{10} helix are usually important to bury the cavity. However, in wild-type *Ss*TrxRB3 the side chain of the residue Gln51 is disordered. This creates a channel which allows movements for the nicotinamide ring and likely favors direct contacts with external solvent. This may facilitate a direct oxidation of NADH by bulk FAD, whose presence is essential for the NADH oxidase activity of *Ss*TrxRB3 [16]. Then, the molecular oxygen regenerates the oxidized FAD molecule from $FADH_2$. In this framework, the marginal NADH oxidase activity of the C147A mutant [16,20] may be ascribed to its high affinity for FAD that prevents NADH binding. In the structure of the complex *Ss*TrxRB3$(NADP)_2$ the 2′ phosphate group of the NADP is located in the active site in the proximity of Glu 46 side chain. The presence of this negatively charged side chain likely reduces the affinity of the protein for NADP. Although the large excess used in the crystallization favored the binding, it can be surmised the strongly reduced oxidase activity exhibited by *Ss*TrxRB3 on the NADPH substrate when compared to the NADH one [16] may be due to a low affinity of the enzyme for NADPH.

Collectively, the present findings may suggest that these novel functions are not related to the presence of the CxxC motif since there is no evidence to support a direct involvement of the redox center of the enzyme in its oxidase activity. Along this line, the inhibition of *Ss*TrxRB3 NADH oxidase activity by reducing agents, such as 2-mercaptoethanol and dithiothreitol [20], may be related to the binding of a FAD molecule at the active site of reduced enzyme that prevents NADH binding and oxidation. These functions may also be associated to other TrxR-like proteins, such as *Ss*TrxRB1 which miss this sequence motif. Sequence alignments indicate that in *Ss*TrxRB1 the CxxC motif is replaced by large amino acids (the local sequence motif is YYTVRRKK). Although structural studies on this enzyme are required to fully clarify this issue, the proximity of this region to the isoalloxazine binding site suggests that it is unlikely that *Ss*TrxRB1 binds FAD in a canonical way.

Denaturation experiments followed by circular dichroism have also provided clues on the structural bases of the thermostability exhibited by the enzyme. In particular, the relatively low $[GuHCl]_{1/2}$ value along with the very high stability of the protein against urea indicate that electrostatic interactions, which are more efficiently weakened by GuHCl, play an important role in the stabilization of *Ss*TrxRB3 [36,38,39]. This finding prompted us to carry out a survey of the electrostatic interactions which may play an important role in the stabilization of *Ss*TrxR. We initially considered the overall content of polar *versus* charged amino acids, since it has been shown that in thermostable protein there is an accumulation of charged residues [40,41]. Our analysis indicate that *Ss*TrxRB3 contains a higher percentage (25.9% *vs* 21.2%) of charged residues (Lys, Arg, Glu, and Asp) and a lower amount (16.1% *vs* 20.5%) of polar residues (Asn, Ser, Gln, and Thr) when compared to the *E. coli* TrxR. This analysis agrees with studies carried out on other hypertermophilic enzymes, that also exhibit a remarkable thermostability [40–42]. The availability of the three-dimensional structure of the protein also offered us the opportunity to identify specific interactions between charged residues [43]. The analysis of the crystal structure of *Ss*TrxRB3 reveals a major cluster of charged residues located at the interface between the FAD-binding domain and the NADP-binding domain of the enzyme (Fig. 11). This network of electrostatic interactions involves four consecutive positively charged residues (Lys124, Arg125, Arg126, and Lys 127),

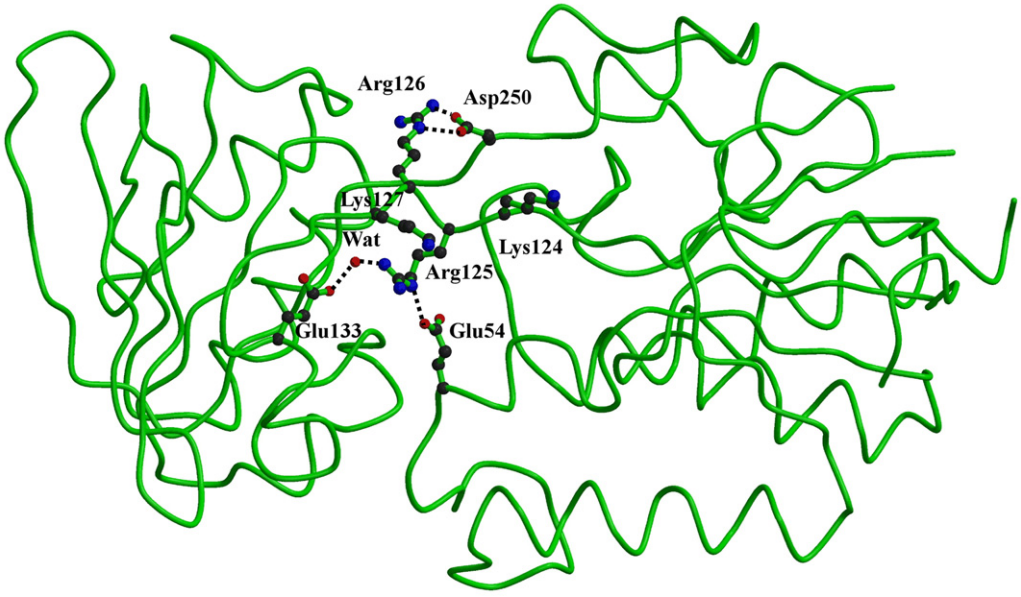

Fig. 11. Cluster of charged side chains identified in the structure of *Ss*TrxRB3. Electrostatic interactions are also shown. Although no clear electron density is detectable for Lys124 and Lys127 side chain atoms beyond the C^{γ}–C^{δ} bond, they are shown to represent the clustering of charged residues in the region.

surrounded by negatively charged residues, which are not present in the sequences of eubacterial/eukaryal Class II TrxR with known structure (Fig. 2). Although the side chain of the lysine residues are partially disordered, the two arginine residues are involved in strong electrostatic interactions (Fig. 11).

In conclusion, the investigations here described provide interesting clues on both structure–function and structure–stability relationships of the enzyme. They also represent a solid base for the definition, at structural level, of the partnerships in the intricate Trx/TrxR/PDO system in *S. solfataricus*.

Acknowledgements

The authors thank the Centro Regionale di Competenza in Diagnostica e Farmaceutica Molecolari for providing some of the facilities used to carry out this work and PRIN 2007-MIUR for financial support. We thank the ESRF Synchrotron (Grenoble, France) for beamtime and the staff of the beam-lines ID14–4 and ID29 for assistance during data collection. The authors also thank Maurizio Amendola and Giosuè Sorrentino for technical assistance and Dr. Vincenzo Granata for the help with the CD spectra registration.

Appendix A. Supplementary data

Supplementary data associated with this article can be found, in the online version, at doi:10.1016/j.bbapap.2008.11.011.

References

[1] G. Bulaj, Formation of disulfide bonds in proteins and peptides, Biotechnol. Adv. 23 (2005) 87–92.
[2] J.M. Thornton, Disulphide bridges in globular proteins, J. Mol. Biol. 151 (1981) 261–287.
[3] M.T. Petersen, P.H. Jonson, S.B. Petersen, Amino acid neighbours and detailed conformational analysis of cysteines in proteins, Protein Eng. 12 (1999) 535–548.
[4] A. De Simone, R. Berisio, A. Zagari, L. Vitagliano, Limited tendency of alpha-helical residues to form disulfide bridges: a structural explanation, J. Pept. Sci. 12 (2006) 740–747.
[5] H. Kadokura, F. Katzen, J. Beckwith, Protein disulfide bond formation in prokaryotes, Annu. Rev. Biochem. 72 (2003) 111–135.
[6] P. Mallick, D.R. Boutz, D. Eisenberg, T.O. Yeates, Genomic evidence that the intracellular proteins of archaeal microbes contain disulfide bonds, Proc. Natl. Acad. Sci. U. S. A. 99 (2002) 9679–9684.
[7] R. Ladenstein, B. Ren, Reconsideration of an early dogma, saying "there is no evidence for disulfide bonds in proteins from archaea", Extremophiles 12 (2008) 29–38.
[8] R. Ladenstein, B. Ren, Protein disulfides and protein disulfide oxidoreductases in hyperthermophiles, FEBS. J. 273 (2006) 4170–4185.
[9] V.Z. Spassov, A.D. Karshikoff, R. Ladenstein, Optimization of the electrostatic interactions in proteins of different functional and folding type, Protein Sci. 3 (1994) 1556–1569.
[10] E.S. Arner, A. Holmgren, Physiological functions of thioredoxin and thioredoxin reductase, Eur. J. Biochem. 267 (2000) 6102–6109.
[11] A.P. Carvalho, P.A. Fernandes, M.J. Ramos, Similarities and differences in the thioredoxin superfamily, Prog. Biophys. Mol. Biol. 91 (2006) 229–248.
[12] A. Argyrou, J.S. Blanchard, Flavoprotein disulfide reductases: advances in chemistry and function, Prog. Nucleic. Acid. Res. Mol. Biol. 78 (2004) 89–142.
[13] R.P. Hirt, S. Muller, T.M. Embley, G.H. Coombs, The diversity and evolution of thioredoxin reductase: new perspectives, Trends Parasitol. 18 (2002) 302–308.
[14] C.H. Williams, L.D. Arscott, S. Muller, B.W. Lennon, M.L. Ludwig, P.F. Wang, D.M. Veine, K. Becker, R.H. Schirmer, Thioredoxin reductase two modes of catalysis have evolved, Eur. J. Biochem. 267 (2000) 6110–6117.
[15] P. Grimaldi, M.R. Ruocco, M.A. Lanzotti, A. Ruggiero, I. Ruggiero, P. Arcari, L. Vitagliano, M. Masullo, Characterisation of the components of the thioredoxin system in the archaeon *Sulfolobus solfataricus*, Extremophiles 12 (2008) 553–562.
[16] M. Masullo, G. Raimo, A. Dello Russo, V. Bocchini, J.V. Bannister, Purification and characterization of NADH oxidase from the archaea *Sulfolobus acidocaldarius* and *Sulfolobus solfataricus*, Biotechnol. Appl. Biochem. 23 (Pt 1) (1996) 47–54.
[17] Q. She, R.K. Singh, F. Confalonieri, Y. Zivanovic, G. Allard, M.J. Awayez, C.C. Chan-Weiher, I.G. Clausen, B.A. Curtis, A. De Moors, G. Erauso, C. Fletcher, P.M. Gordon, I. Heikamp-de Jong, A.C. Jeffries, C.J. Kozera, N. Medina, X. Peng, H.P. Thi-Ngoc, P. Redder, M.E. Schenk, C. Theriault, N. Tolstrup, R.L. Charlebois, W.F. Doolittle, M. Duguet, T. Gaasterland, R.A. Garrett, M.A. Ragan, C.W. Sensen, J. Van der Oost, The complete genome of the crenarchaeon *Sulfolobus solfataricus* P2, Proc. Natl. Acad. Sci. U. S. A. 98 (2001) 7835–7840.
[18] E. Pedone, D. Limauro, R. D'Alterio, M. Rossi, S. Bartolucci, Characterization of a multifunctional protein disulfide oxidoreductase from *Sulfolobus solfataricus*, FEBS J. 273 (2006) 5407–5420.
[19] P. Arcari, L. Masullo, M. Masullo, F. Catanzano, V. Bocchini, A NAD(P)H oxidase isolated from the archaeon *Sulfolobus solfataricus* is not homologous with another NADH oxidase present in the same microorganism. Biochemical characterization of the enzyme and cloning of the encoding gene, J. Biol. Chem. 275 (2000) 895–900.
[20] M.R. Ruocco, A. Ruggiero, L. Masullo, P. Arcari, M. Masullo, A 35 kDa NAD(P)H oxidase previously isolated from the archaeon *Sulfolobus solfataricus* is instead a thioredoxin reductase, Biochimie 86 (2004) 883–892.
[21] A. Ruggiero, M.R. Ruocco, P. Grimaldi, P. Arcari, M. Masullo, A. Zagari, L. Vitagliano, Crystallization and preliminary X-ray crystallographic analysis of *Sulfolobus solfataricus* thioredoxin reductase, Acta Crystallogr. F61 (2005) 906–909.
[22] T.C. Terwilliger, SOLVE and RESOLVE: automated structure solution and density modification, Methods Enzymol. 374 (2003) 22–37.
[23] K.D. Cowtan, K.Y. Zhang, Density modification for macromolecular phase improvement, Prog. Biophys. Mol. Biol. 72 (1999) 245–270.
[24] A. Perrakis, R. Morris, V.S. Lamzin, Automated protein model building combined with iterative structure refinement, Nat. Struct. Biol. 6 (1999) 458–463.
[25] A.T. Brunger, Version 1.2 of the crystallography and NMR system, Nat. Protoc. 2 (2007) 2728–2733.
[26] T.R. Schneider, A.T. Brunger, M. Nilges, Influence of internal dynamics on accuracy of protein NMR structures: derivation of realistic model distance data from a long molecular dynamics trajectory, J. Mol. Biol. 285 (1999) 727–740.
[27] T.A. Jones, J.Y. Zou, S.W. Cowan, M. Kjeldgaard, Improved methods for building protein models in electron density maps and the location of errors in these models, Acta Crystallogr. A47 (1991) 110–119.
[28] G. Waksman, T.S. Krishna, C.H. Williams Jr, J. Kuriyan, Crystal structure of *Escherichia coli* thioredoxin reductase refined at 2 A resolution. Implications for a large conformational change during catalysis, J. Mol. Biol. 236 (1994) 800–816.
[29] M. Akif, K. Suhre, C. Verma, S.C. Mande, Conformational flexibility of *Mycobacterium tuberculosis* thioredoxin reductase: crystal structure and normal-mode analysis, Acta Crystallogr. D61 (2005) 1603–1611.
[30] B.W. Lennon, C.H. Williams Jr, M.L. Ludwig, Crystal structure of reduced thioredoxin reductase from *Escherichia coli*: structural flexibility in the isoalloxazine ring of the flavin adenine dinucleotide cofactor, Protein Sci. 8 (1999) 2366–2379.
[31] B.W. Lennon, C.H. Williams Jr, M.L. Ludwig, Twists in catalysis: alternating conformations of Escherichia coli thioredoxin reductase, Science 289 (2000) 1190–1194.
[32] S. Dai, M. Saarinen, S. Ramaswamy, Y. Meyer, J.P. Jacquot, H. Eklund, Crystal structure of *Arabidopsis thaliana* NADPH dependent thioredoxin reductase at 2.5 A resolution, J. Mol. Biol. 264 (1996) 1044–1057.
[33] T.N. Gustafsson, T. Sandalova, J. Lu, A. Holmgren, G. Schneider, High-resolution structures of oxidized and reduced thioredoxin reductase from *Helicobacter pylori*, Acta Crystallogr. D63 (2007) 833–843.
[34] O. Dym, D. Eisenberg, Sequence-structure analysis of FAD-containing proteins, Protein Sci. 10 (2001) 1712–1728.
[35] A. Lobley, L. Whitmore, B.A. Wallace, DICHROWEB: an interactive website for the analysis of protein secondary structure from circular dichroism spectra, Bioinformatics 18 (2002) 211–212.
[36] J.K. Myers, C.N. Pace, J.M. Scholtz, Denaturant m values and heat capacity changes: relation to changes in accessible surface areas of protein unfolding, Protein Sci. 4 (1995) 2138–2148.
[37] M. Beeby, B.D. O'Connor, C. Ryttersgaard, D.R. Boutz, L.J. Perry, T.O. Yeates, The genomics of disulfide bonding and protein stabilization in thermophiles, PLoS Biol. 3 (2005) e309.
[38] V. Granata, G. Graziano, A. Ruggiero, G. Raimo, M. Masullo, P. Arcari, L. Vitagliano, A. Zagari, Stability against temperature of *Sulfolobus solfataricus* elongation factor 1 alpha, a multi-domain protein, Biochim. Biophys. Acta 1784 (2008) 573–581.
[39] V. Granata, G. Graziano, A. Ruggiero, G. Raimo, M. Masullo, P. Arcari, L. Vitagliano, A. Zagari, Chemical denaturation of the elongation factor 1alpha isolated from the hyperthermophilic archaeon *Sulfolobus solfataricus*, Biochemistry 45 (2006) 719–726.
[40] C. Cambillau, J.M. Claverie, Structural and genomic correlates of hyperthermostability, J. Biol. Chem. 275 (2000) 32383–32386.
[41] G.I. Makhatadze, V.V. Loladze, A.V. Gribenko, M.M. Lopez, Mechanism of thermostabilization in a designed cold shock protein with optimized surface electrostatic interactions, J. Mol. Biol. 336 (2004) 929–942.
[42] K. Suhre, J.M. Claverie, Genomic correlates of hyperthermostability, an update, J. Biol. Chem. 278 (2003) 17198–17202.
[43] A. Karshikoff, R. Ladenstein, Ion pairs and the thermotolerance of proteins from hyperthermophiles: a "traffic rule" for hot roads, Trends Biochem. Sci. 26 (2001) 550–556.